JAAS

ROYAL SOCIETY OF CHEMISTRY

PAPER

View Article Online
View Journal | View Issue

Cite this: *J. Anal. At. Spectrom.*, 2025, **40**, 2937

Non-linearity correction for variable signal analysis in mass spectrometry using discrete ion counters

Stefaan Pommé *

The response of a discrete ion counter is not perfectly linear due to count loss caused by dead time and pulse pileup. As a result, the output rate of the counter does not scale linearly with the input rate of ions reaching the detector. The value of a stable input rate can be determined from the measured output rate by inverting the throughput formula of the ion counter. However, when the input rate varies during the measurement, a mismatch between the average input rate and the average output rate becomes apparent. The resulting bias can be particularly significant when measuring transient signals. A correction procedure is proposed to calculate a better estimate of the average input rate from the observed mean and variance of the output rate. Implementation of this refined throughput formula is recommended to improve accuracy of mass spectrometry utilising discrete ion counters.

Received 20th June 2025
Accepted 15th July 2025

DOI: 10.1039/d5ja00243e

rsc.li/jaas

1 Introduction

In mass spectrometry,[1] the choice between using Faraday cups or discrete ion counters (such as electron multipliers, microchannel plates, or Daly detectors) for ion detection depends on various factors, including the abundance ratios of the isotopes being measured, the sensitivity required, and the dynamic range of the measurements. Faraday cups are typically used for measuring high abundance ratios, where the signal intensity is relatively high, and the signal-to-noise ratio is less critical. Faraday cups provide a direct measurement of the total ion current passing through the detector without the need for signal amplification. On the other hand, discrete ion counters are often employed for measuring low abundance ratios, where the signal intensity is low, and high sensitivity and amplification are required for accurate ion detection. These detectors have a fast response time and are advantageous in processing a wide dynamic range of signal intensities.

The linearity of the counting process in a discrete ion counter is affected by count loss due to "pulse pileup" and "non-extending dead time".[2–4] It is common practice to impose a factory-set non-extending dead time on each counted event, which exceeds the width of the electronic pulses generated by the ion detector.[5–9] This dead-time setting helps suppress the effect of pulse pileup across a wide input range. However, at extremely high input rates, pulse pileup will emerge as a notable contributor to count loss.[10–14] This process can be accurately predicted by an advanced EDT–NEDT throughput model that reflects the interplay between extending (EDT) and non-extending dead time (NEDT).[2–4] Pommé and Boulyga recently published an overview of relevant formulas for the throughput curve of discrete ion counters, the inverted throughput function to correct for count loss, the resulting counting uncertainty, the error propagation of the characteristic dead time and pulse width, and the error made by incomplete count-loss correction when ignoring pileup.[2] This approach enables extending the linearity of the ion counter across the full range of input rates, thus mitigating rate-related bias in mass spectrometry.

Existing literature provides explicit evidence that current practice in mass spectrometry encounters limitations in dynamic range of discrete ion counters at high count rates.[10] Already in 2002, Nomizu *et al.*[11] pointed to the limited linearity of the channel electron multiplier in pulse-counting mode when observing non-linear response for the analysis of airborne Zn particles. Olesik and Gray[12] considered various explanations for a limited dynamic range in analysing microparticles by single-particle inductively coupled plasma mass spectrometry (spICP-MS), including incomplete ionisation of particles, local plasma cooling, and competing rates of particle vaporisation and diffusion of ions. However, they also emphasised the importance of the "dead time" near the peak of transient signals. Strenge and Engelhard[13] observed nonlinear response in pulse counting mode in spICP-MS and investigated the suitability of the traditional dead-time correction method (DTC) in millisecond and microsecond time-resolved spICP-MS. By applying DTC in each time channel, they managed to extend the linear dynamic range a bit further. Lomax-Vogt *et al.*[14] have identified pulse pileup as a limiting factor for the maximum intensity that can be accurately measured in pulse counting mode by single-particle ICRP-QMS (typically 2 million counts per second, or about 200 counts per 0.1 ms). This limits the acceptable size of nanoparticles that can be analysed, which can be extended marginally if classical DTC is applied. In a forthcoming paper, Siegmund *et al.*[15] report on a linearity test of secondary electron multipliers (SEM) subjected to a $^{233}U/^{235}U$

European Commission, Joint Research Centre (JRC), Geel, Belgium. E-mail: stefaan.pomme@ec.europa.eu; Tel: +32 (0)14 571 289

beam at input fluxes from *ca.* 10^4 to about 3×10^7 ions per second. The results confirm that the diminishing response of the ion detection system at ion fluxes above 2×10^6 s^{-1} is compatible with the theoretical throughput formula published by Pommé and Boulyga.[2]

The EDT-NEDT throughput model successfully solves the non-linearity problem for measurements of a "stationary Poisson process", where the input rate ρ of events (ions impacting the sensitive area of the ion counter) remains constant during the measurement. However, another non-linearity effect lurks around the corner when the input rate undergoes substantial changes during the measurement. Since the output rate does not vary linearly with the input rate, a conventional dead time correction over the average output rate will not result in the corresponding average input rate.[16–19] This may cause a significant bias in the measurement result, particularly for transient signals. This paper explains the mechanism causing the non-linearity phenomenon and presents a correction method that reduces the error substantially.

To establish a clear understanding of this secondary non-linearity effect, the mathematical derivations are conducted using simple scenarios involving linear or exponential changes in beam intensity over time. These conditions are not limited to slowly fluctuating count rates over extended measurement durations but also encompass short-term intervals, where *e.g.* transient signals are sampled through time-resolved mass spectrometry at ultra-short time scales.[20–26] In the latter case, the perceived count rate will depend on the dwell time.[26] The significance of the non-linearity bias will be examined through numerical examples across a range of count rates and varying levels of input rate variance. While the correction formula developed in this work is broadly applicable to signal shapes of various types, including transient signals conforming approximately to normal or log-normal distributions over time,[27,28] the exploration of more intricate mathematical models is best suited for a subsequent publication.

2 Throughput at fixed rate

Radionuclide metrologists[29,30] have extensively researched the impact of pulse pileup, extending dead time (EDT), and non-extending dead time (NEDT) on the throughput of nuclear counters with the aim of improving the accuracy of radioactivity measurements.[2–4,31–53] The resulting theories are also relevant to ion counting in mass spectrometry. A key prerequisite is that the input process conforms to a "stationary Poisson process", implying a constant input event rate, ρ, of ions impacting the sensitive area of the ion counter, with ions arriving randomly in time following exponentially distributed time intervals.

In current practice, the primary source of dead time in mass spectrometers is the factory-set NEDT of duration τ_{ne} imposed on observed events from the pulse amplifier. This dead time is

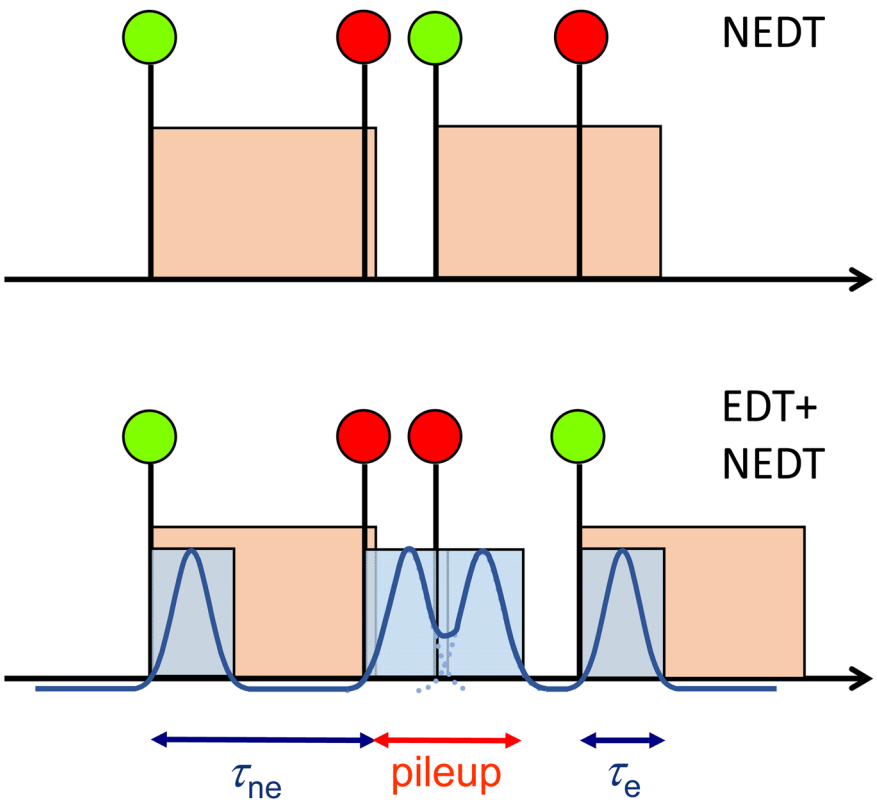

Fig. 1 (Top) Simplified model commonly used to describe count loss in ion counters. NEDT is imposed on counted events (green dot) and other events falling in the NEDT period are ignored (red dot). (Bottom) More realistic EDT + NEDT model accounting for finite pulse width. A pulse is identified when it rises above a threshold level. Effective dead time can be extended through pileup of pulses, since the sum pulse is identified as a single event.

triggered when the leading edge of a pulse surpasses the discriminator threshold. Any subsequent pulse arriving within the NEDT window is not counted, and prolongation of the dead-time period through pulse pileup is ignored (see Fig. 1). The throughput formula for a purely NEDT-based counter is:[4,31]

$$R = \rho X(\rho) = \frac{\rho}{1 + \rho\tau_{ne}} \quad (1)$$

in which $X(\rho)$ represents the rate-dependent throughput factor, ρ is the input rate, and τ_{ne} is the characteristic dead time.

When observing a count rate R, the throughput formula must be inverted to calculate a best estimate $\hat{\rho}$ of the original input rate. The following inverse throughput formula is commonly used in mass spectrometry to compensate for count loss attributed to NEDT:[4–9,31]

$$\hat{\rho} = RX^{-1}(R) = \frac{R}{1 - R\tau_{ne}} \quad (2)$$

in which $X^{-1}(R)$ represents the inverse throughput factor for NEDT.

The formulas in eqn (1) and (2) are valid only by approximation, mainly in a region where the input rate is not excessively high. In reality, the pulses of the detector have a finite width, and the overlap of neighbouring pulses results in additional count loss. This count loss mechanism can be modelled as a Poisson process passing through EDT and NEDT in series[2–4,31–33,43] (see Fig. 1). Mathematical formulas are available for the time-interval distribution of counted events, the expected throughput rate, and the counting uncertainty for such system.[2–4,31] The appropriate throughput formula applicable to ion counters in mass spectrometry is:

$$R = \rho X(\rho) = \frac{\rho}{e^{\rho\tau_e} + \rho_{max}\{0, \tau_{ne} - \tau_e\}}$$
$$\xrightarrow[\tau_{ne} > \tau_e]{} R = \frac{\rho}{e^{\rho\tau_e} + \rho(\tau_{ne} - \tau_e)} \quad (3)$$

The second version of the formula generally applies, because the NEDT is purposely chosen by the manufacturer to exceed the pulse width, *i.e.* $\tau_{ne} > \tau_e$.

Inversion of eqn (3) is less straightforward than the case of NEDT (eqn (2)), and has in principle two solutions, one for $\rho\tau_e \leq 1$ and another for $\rho\tau_e \geq 1$. The solution at moderate input rates, $\rho_< < 1/\tau_e$, can be obtained in a few iterations through the following recursion formula:[2–4]

$$\hat{\rho}_< = RX^{-1}(R) = \frac{R}{1 - R\tau_{ne}}\{e^{\hat{\rho}_<\tau_e} - \hat{\rho}_<\tau_e\} \quad (4)$$

Alternatively, even faster iterations can be obtained from the Newton–Raphson method:[2]

$$\hat{\rho}_< = \hat{\rho} + \frac{(\hat{\rho} - Rz)z}{e^{\hat{\rho}_<\tau_e}(\hat{\rho}_<\tau_e - 1)} \quad (5)$$

where $z = e^{\hat{\rho}\tau_e} + \hat{\rho}(\tau_{ne} - \tau_e)$ and eqn (2) can be used as a starting point. The second solution, $\rho_> > 1/\tau_e$, requires another formula for the starting value.[2]

For a stationary Poisson process, there is a unique relationship between the (moderate) input rate and the output rate. One can be converted into the other through $R = \rho X(\rho)$ and $\rho = RX^{-1}(R)$ without ambiguity, provided that the dead-time parameters τ_{ne} and τ_e are accurately known.

3 Throughput at variable rate

In actual mass spectrometry measurements, the count rate may fluctuate slightly, at the percent level, or by more significant amounts. When fluctuations are minor, inverting the average output rate, $\hat{\rho} = \bar{R}X^{-1}(\bar{R})$, can still provide a sufficiently accurate estimate of the average input rate, $\bar{\rho}$. This holds particularly true at low count rates, where the throughput function is quasi-linear, ensuring that $\bar{\rho}$ and $\bar{R}$ vary proportionally. However, a substantial deviation from this ideal scenario can be anticipated at high input rates and in the presence of significant fluctuations. Such conditions are common in, for example, analysis of single nanoparticles or ablated aerosol particles in inductively-coupled plasma mass spectrometry (ICPMS).[11–14,27,28] Where the throughput curve is bent, there will be a mismatch between the average input and output rates, $\bar{R}X^{-1}(\bar{R}) \neq \bar{\rho}$ and $\bar{\rho}X(\bar{\rho}) \neq \bar{R}$, as demonstrated for an extreme case in Fig. 2.

Failing to correct for this non-linearity will introduce a bias in measured isotopic abundance ratios. This error can be significantly reduced by including a correction term within the throughput formula. It suffices to consider the simple scenario where the count rate varies linearly between two extreme values, ρ_{min} and ρ_{max}. While the mean input rate is simply $\bar{\rho} = (\rho_{max} + \rho_{min})/2$, determining the mean output rate requires integrating the throughput factor. This mathematical problem can be simplified by approximating the throughput curve in the considered interval $[\rho_{min}, \rho_{max}]$ by a parabola:

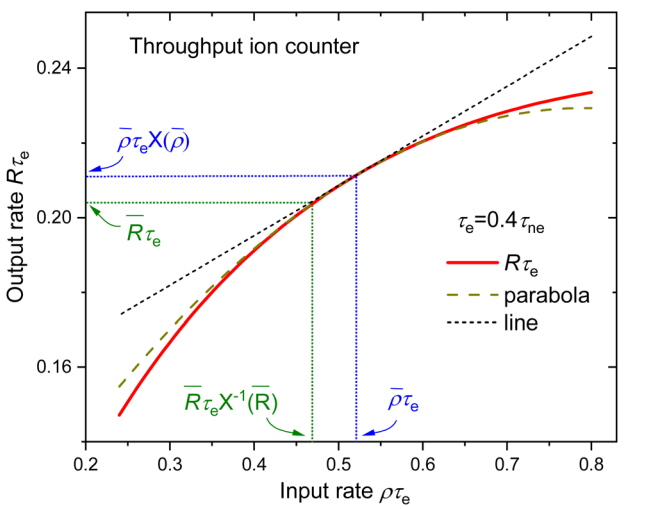

Fig. 2 Throughput curve (full line) of an ion counter with τ_e = 20 ns, τ_{ne} = 50 ns, covering a region where the input rate varies by 70% between 1.2 10^7 s^{-1} and 4 10^7 s^{-1}. The dotted lines show the tangent (first derivative) and matching parabola (first and second derivative). There is a mismatch between the projections of $\bar{\rho}$ and $\bar{R}$ over this region.

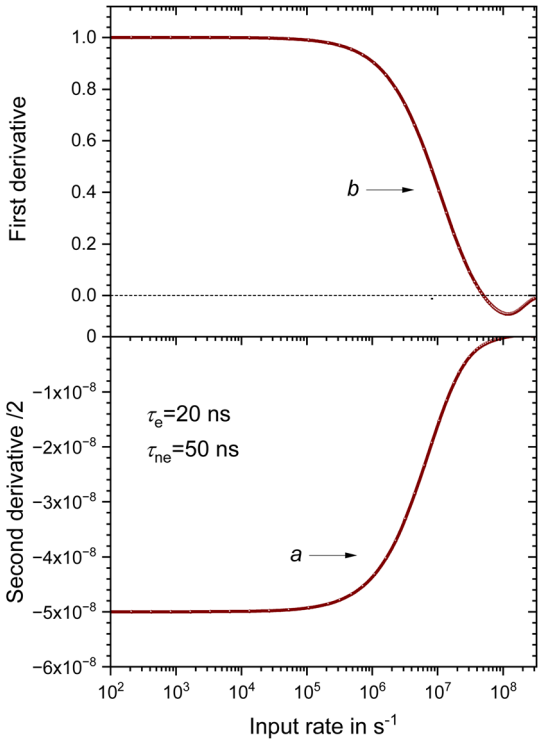

Fig. 3 Plot of the parameters b and a, proportional to the first and second derivatives of the throughput formula, $R = \rho X(\rho)$, of an ion counter with $\tau_e = 20$ ns, $\tau_{ne} = 50$ ns.

$$R(\rho) \approx a\rho^2 + b\rho \tag{6}$$

where the matching coefficients can be derived from a Taylor expansion:

$$b = \frac{\partial R}{\partial \rho} = \frac{e^{\rho\tau_e}(1-\rho\tau_e)}{[e^{\rho\tau_e} + \rho(\tau_{ne}-\tau_e)]^2} \tag{7}$$

and

$$a = \frac{1}{2}\frac{\partial^2 R}{\partial \rho^2} = \frac{-b}{2\rho}\left[\frac{(\rho\tau_e)^2}{1-\rho\tau_e} + 2\frac{\rho\tau_e e^{\rho\tau_e} + \rho(\tau_{ne}-\tau_e)}{e^{\rho\tau_e} + \rho(\tau_{ne}-\tau_e)}\right] \tag{8}$$

Typical values of a and b at various input rates are presented in Fig. 3.

The mean output rate is then obtained from an integral:

$$\begin{aligned}\overline{R} &\approx \frac{1}{(\rho_{max}-\rho_{min})}\int_{\rho_{min}}^{\rho_{max}} (a\rho^2 + b\rho)\mathrm{d}\rho \\ &= \frac{1}{(\rho_{max}-\rho_{min})}\left[\frac{a\rho^3}{3} + \frac{b\rho^2}{2}\right]\Bigg|_{\rho_{min}}^{\rho_{max}} \\ &= a\frac{(\rho_{min}^2 + \rho_{min}\rho_{max} + \rho_{max}^2)}{3} + b\frac{(\rho_{min}+\rho_{max})}{2} \\ &= a\overline{\rho}^2 + b\overline{\rho} + a\frac{(\rho_{max}-\rho_{min})^2}{12}\end{aligned} \tag{9}$$

The last term contains the variance of the input rate, which has a rectangular distribution. The solution in eqn (9) can be generalised to a new throughput formula applicable to any normalised statistical distribution $f(\rho)$ of the input rate:

$$\begin{aligned}\overline{R} &\approx \int f(\rho)(b\rho + a\rho^2)\mathrm{d}\rho \\ &= a\overline{\rho}^2\int f(\rho)\mathrm{d}\rho + b\int f(\rho)\rho\mathrm{d}\rho + a\int f(\rho)(\rho^2 - \overline{\rho}^2)\mathrm{d}\rho \\ &\approx \overline{\rho}X(\overline{\rho}) + a\sigma_\rho^2\end{aligned} \tag{10}$$

The error caused by fluctuations in the count rate is proportional to the variance of the input rate and half the second derivative of the throughput function. Since the second derivative of the throughput curve is negative ($a < 0$), the average count rate will be lower than expected from the stationary throughput formula in eqn (3), *i.e.* $\bar{R} < \bar{\rho}X(\bar{\rho})$. These conclusions are compatible with observations in other fields of research, such as *e.g.* photon counting from a fluctuating light beam.[16–19] Eqn (10) offers an elegant and broadly applicable solution to the expected change in average count rate. Other authors have also explored the impact of input fluctuations on the distribution and variance of counts.[16–19]

4 Inverse throughput at variable rate

From an experimental perspective, conducting measurements at variable rates will result in average output rates $\bar{R}$ that align with eqn (10). Inversion of the throughput formula will yield an underestimate of the average input rate, $\hat{\rho} = \bar{R}X^{-1}(\bar{R}) \leq \bar{\rho}$, leading to a bias in isotopic abundance ratios. Since the error term in $\bar{R}$ is relatively small, it can be translated into a variation in $\bar{\rho}$ by using the inverse of the first derivative of $X(\bar{\rho})$, which is $1/b$:

$$\overline{\rho} \approx \overline{R}X^{-1}\left(\overline{R}\right) - \frac{a}{b}\sigma_\rho^2 \tag{11}$$

As the experimenter cannot directly observe the variance of the input rate, σ_ρ^2, it must be estimated from the variance of the output rate, σ_R^2. Again, a linear relationship between both standard deviations or a quadratic one between the variances, $\sigma_R^2 \approx b^2\sigma_\rho^2$, can serve as a suitable approximation. This leads to the following refinement of the inverse throughput formula:

$$\overline{\rho} \approx \hat{\rho}_< - \frac{a}{b}\frac{\sigma_R^2}{b^2} \tag{12}$$

The first term, $\hat{\rho}_< = \bar{R}X^{-1}(\bar{R})$, follows from iteratively solving eqn (4) or (5). Then local values for the first and second derivatives forming a and b are calculated locally for $\hat{\rho}_<$ and an estimate for $\bar{\rho}$ is calculated from eqn (12). A generally unnecessary next step would consist of another iteration of eqn (12) in which new values of a and b are determined using the obtained estimate of $\bar{\rho}$. Eqn (12) is applicable to virtually all mass spectrometry measurements utilising discrete ion counters. It is unnecessary for systems that are inherently linear ($a = 0$), such

as current measurements in a Faraday cup. By incorporating this universal throughput formula into the data processing software as a standard procedure, the accuracy of abundance ratios is generally expected to improve.

5 Exponential variation

Whereas the correction factor in eqn (9) pertains to a linear change of the input rate, it is also a very good approximation for an exponential variation of the input rate, for example due to evaporation of the sample at a rate $-\lambda$. The mean input rate is slightly lower than for a rectangular distribution:

$$\bar{\rho} = \rho_{\max} \frac{1 - e^{-\lambda T}}{\lambda T} \tag{13}$$

in which $\lambda T = \ln(\rho_{\max}/\rho_{\min}) \approx (\rho_{\max} - \rho_{\min})/\bar{\rho}$. The variance divided by the squared mean of the exponential distribution is

$$\frac{\sigma_\rho^2}{\bar{\rho}^2} = \left(\frac{1 - e^{-2\lambda T}}{2\lambda T}\right) \Big/ \left(\frac{1 - e^{-\lambda T}}{\lambda T}\right)^2 - 1$$

$$\approx \frac{(\lambda T)^2}{12} \approx \frac{1}{\bar{\rho}^2} \frac{(\rho_{\max} - \rho_{\min})^2}{12} \tag{14}$$

The relative variation of the exponentially-distributed input rate is well approximated by the same formula as for the linear distribution, albeit that the mean value $\bar{\rho}$ from eqn (13) is slightly lower than $(\rho_{\max} + \rho_{\min})/2$. Consequently, $(\rho_{\max} - \rho_{\min})^2/12$ can be used as variance in eqn (10) for an accurate prediction of the output rate (with $\bar{\rho}$ from eqn (13)), and in eqn (11) and (12) to improve the input rate estimation.

6 Numerical examples

Numerical examples are provided in Table 1 and visualised in Fig. 4. An ion counter is modelled with a characteristic pulse width of $\tau_e = 20$ ns and an imposed NEDT of $\tau_{ne} = 50$ ns. Table 1 shows a series of input rates that vary linearly during measurement, their rectangular distribution being characterised by the average value, $\bar{\rho}$, and relative width, $(\rho_{\max} - \rho_{\min})/\bar{\rho}$. For each hypothetical measurement, the relative error on the estimated count rate, $\hat{\rho}/\bar{\rho} - 1$, is presented. The errors can be effectively reproduced through eqn (12), even when approximating the output rate variance with that of a rectangular distribution:

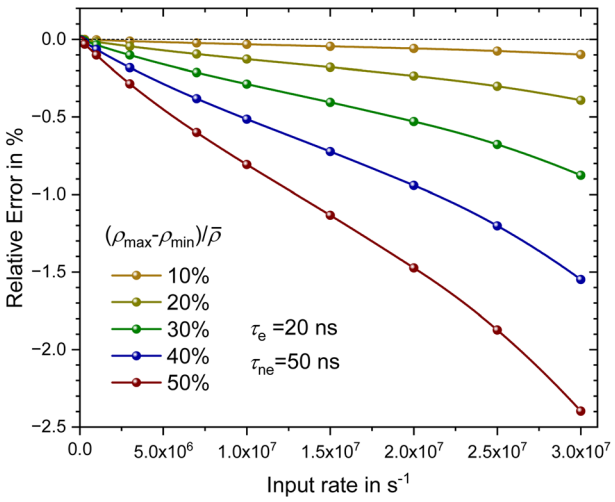

Fig. 4 Relative error on the calculated average input rate by inverting the throughput curve for different widths of the input rate distribution during the measurement in an ion counter with $\tau_e = 20$ ns, $\tau_{ne} = 50$ ns. Note that the width of the output rate distribution will appear smaller by a factor of b.

$$\frac{a}{b}\sigma_\rho^2 \approx \frac{a}{b} \frac{(R_{\max} - R_{\min})^2}{12b^2} \tag{15}$$

The statistical significance of the calculated errors should be evaluated by comparing them with the claimed accuracy of measurement results. By remarkably good approximation (relative difference <2%), the same relative errors apply to a scenario with an exponential variation of the input rates.

7 Time-resolved transient

Another numerical example pertains to conducting a time-resolved analysis of a Gaussian-shaped transient signal. It

Table 1 Evaluation of relative error in estimated average input rate for linearly varying input rates between $\rho_{\max}$ and $\rho_{\min}$. The values represent the relative error, $\hat{\rho}/\bar{\rho} - 1$, by inversion of the throughput formula, $\hat{\rho} = \bar{R}X^{-1}(\bar{R})$, for an ion counter with pulse width $\tau_e = 20$ ns and NEDT $\tau_{ne} = 50$ ns, as a function of the average input rate and the relative width of the interval in which the input rate varies

	$\hat{\rho}/\bar{\rho} - 1$ *versus* $\bar{\rho}$ and $(\rho_{\max} - \rho_{\min})/\bar{\rho}$				
$\bar{\rho}$	10%	20%	30%	40%	50%
1.00×10^5	−0.00042%	−0.0017%	−0.0037%	−0.0066%	−0.0104%
3.00×10^5	−0.0012%	−0.0049%	−0.011%	−0.020%	−0.031%
1.00×10^6	−0.0040%	−0.016%	−0.036%	−0.064%	−0.100%
3.00×10^6	−0.0113%	−0.045%	−0.102%	−0.18%	−0.28%
7.00×10^6	−0.0237%	−0.095%	−0.213%	−0.38%	−0.59%
1.00×10^7	−0.032%	−0.128%	−0.29%	−0.51%	−0.80%
1.50×10^7	−0.045%	−0.180%	−0.40%	−0.72%	−1.12%
2.00×10^7	−0.059%	−0.235%	−0.53%	−0.94%	−1.47%
2.50×10^7	−0.075%	−0.302%	−0.68%	−1.20%	−1.88%
3.00×10^7	−0.098%	−0.39%	−0.88%	−1.6%	−2.4%

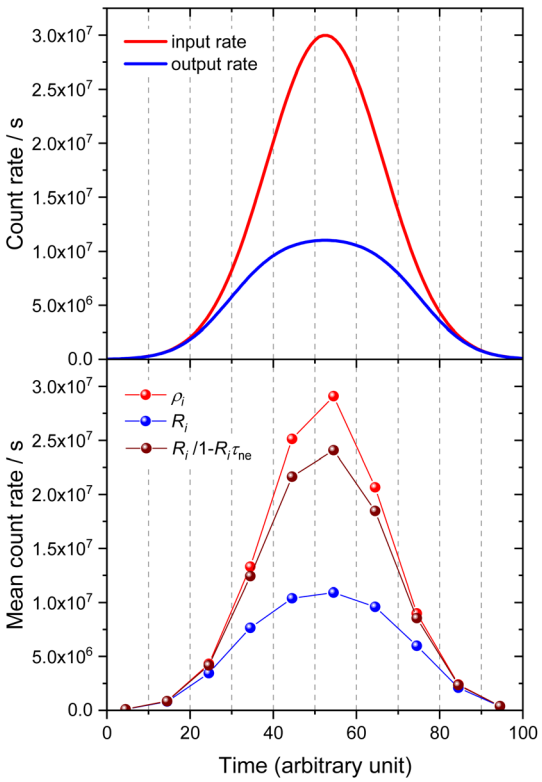

Fig. 5 (Top) Transient signal with Gaussian shape and corresponding output rate in a discrete counter with $\tau_e = 20$ ns, $\tau_{ne} = 50$ ns. (Bottom) Time-resolved input and output count rates averaged over finite time intervals indicated by vertical dashed lines, and the dead-time corrected count rate based on the NEDT model in eqn (2).

bares resemblance to a measurement result published by Strenge and Engelhard,[20] who recorded 0.2 ms transient signals with 5 μs time resolution. The output rate reached values near 60 counts per 5 μs (equivalent to 1.2×10^7 s^{-1}), which corresponded to estimated input rates as high as 140 counts per 5 μs (or 2.8×10^7 s^{-1}) after dead-time correction. The authors applied the default dead-time correction method outlined in eqn (2) for each time interval to mitigate count loss in the spike's count integral. At such elevated count rates, the throughput formula significantly diverges from the NEDT formula in eqn (1), necessitating the adoption of eqn (3) for a cascade of EDT-NEDT instead.

For the sake of illustration, the dwell time in the numerical example is chosen to be about 1/10th of the width of the Gaussian spike, as shown in Fig. 5. Consequently, the average count rate exhibits variability within each time interval, which can be approximated by comparing the average count rates in neighbouring time intervals:

$$\sigma_{R_i}^2 \approx \frac{1}{12}\left(\frac{|R_i - R_{i-1}| + |R_{i+1} - R_i|}{2}\right)^2 \quad (16)$$

in which i is the index number of the time interval. Alternative formulas for the variance have been derived, *e.g.*

$$\sigma_{R_i}^2 \approx \frac{1}{12}\left(\frac{\max(R_{i-1}, R_i, R_{i+1}) - \min(R_{i-1}, R_i, R_{i+1})}{2}\right)^2 \quad (17)$$

or, based on a parabolic fit to three data:

$$\sigma_{R_i}^2 \approx \frac{1}{12}\left(\frac{R_{i+1} - R_{i-1}}{2}\right)^2 + \frac{17}{1440}\left(\frac{R_{i+1} + R_{i-1}}{2} - R_i\right)^2 \quad (18)$$

but in numerical tests of the integral error, eqn (16) appeared the most successful in combination with eqn (15).

In Table 2, the input and output rates of the Gaussian spike are averaged in each interval. Starting from the output rates R_i, estimates of the input rates ρ_i are calculated using three approaches: (1) $\hat{\rho}_i^{(1)}$ = the NEDT inverse throughput formula in eqn (2), (2) $\hat{\rho}_i^{(2)}$ = the static EDT-NEDT formula in eqn (5), and (3) $\hat{\rho}_i^{(3)}$ = the variance-corrected EDT–NEDT formula in eqn (12). For a Gaussian with peak input rate of 3×10^7 s^{-1} while $\tau_e = 20$ ns and NEDT $\tau_{ne} = 50$ ns, the error in reproducing the count integral associated with the three methods are (1) −12%, (2) −1.6%, and (3) −0.1%, respectively. The biggest gain in accuracy is achieved by accounting for the pileup effect. Accounting for the count rate variance within each channel can further reduce the remaining error by another order of magnitude, depending on the dwell time of the spectrometer.

Table 2 Time-resolved analysis of a Gaussian-shaped transient signal using a discrete ion counter with $\tau_e = 20$ ns and NEDT $\tau_{ne} = 50$ ns. The data refer to the (i) hypothetical time intervals, (ii) the average input rate and (iii) output rate in each time range, (iv) the estimated output-rate variance from eqn (16), the estimated input rate based on the inverse throughput formulas in (v) eqn (2), (vii) eqn (5) and (ix) eqn (12), and (vi) (viii) (x) the corresponding relative differences with the real input rate

Time range	ρ_i	R_i	$\sigma_{R_i}^2$	$\hat{\rho}_i^{(1)}$	Error	$\hat{\rho}_i^{(2)}$	Error	$\hat{\rho}_i^{(3)}$	Error
0–9	1.04×10^5	1.03×10^5	1.35×10^{10}	1.04×10^5	−0.2%	1.04×10^5	−0.2%	1.04×10^5	0.4%
10–19	8.56×10^5	8.12×10^5	2.34×10^{11}	8.46×10^5	−1.2%	8.46×10^5	−1.1%	8.60×10^5	0.4%
20–29	4.31×10^6	3.45×10^6	9.79×10^{11}	4.18×10^6	−3.2%	4.19×10^6	−2.9%	4.28×10^6	−0.7%
30–39	1.33×10^7	7.67×10^6	1.00×10^{12}	1.24×10^7	−6.5%	1.29×10^7	−3.2%	1.32×10^7	−0.8%
40–49	2.51×10^7	1.04×10^7	2.21×10^{11}	2.16×10^7	−13.8%	2.48×10^7	−1.2%	2.51×10^7	0.1%
50–59	2.91×10^7	1.09×10^7	7.13×10^{10}	2.41×10^7	−17.3%	2.91×10^7	−0.1%	2.92×10^7	0.5%
60–69	2.07×10^7	9.60×10^6	5.07×10^{11}	1.85×10^7	−10.6%	2.02×10^7	−2.2%	2.06×10^7	−0.2%
70–79	8.99×10^6	5.99×10^6	1.17×10^{12}	8.55×10^6	−4.9%	8.69×10^6	−3.4%	8.90×10^6	−1.0%
80–89	2.40×10^6	2.10×10^6	6.56×10^{11}	2.34×10^6	−2.3%	2.34×10^6	−2.2%	2.39×10^6	−0.2%
90–99	3.91×10^5	3.81×10^5	8.92×10^{10}	1.42×10^5	−0.3%	1.42×10^5	−0.3%	1.43×10^5	0.6%
Integral					−12%		−1.6%		−0.1%

8 Conclusion

The throughput factor in eqn (3) quantifies the relationship between a constant input rate of ions entering an ion counter and the resulting output rate, which is affected by count loss through dead time and pulse pileup. However, when the input rates exhibit significant variations during measurement, the throughput formula has to be refined as outlined in eqn (9) and (10), with a correction factor to account for the non-linearity between the average input and output rates. Table 1 provides examples of anticipated relative errors, applicable to scenarios where the input rates vary linearly or exponentially by 10% to 50%. Table 2 shows similar errors in time-resolved analysis of a Gaussian-shaped transient signal. In such instances, it suffices to calculate the variance of the output rate from its extreme values using eqn (15) and to propagate this variance to derive an unbiased input rate using eqn (12). As a result, the linearity of discrete ion counters can be improved for varying beam intensities, and bias in mass spectrometry measurement with discrete ion counters can be mitigated.

Data availability

All data in Tables and graphs have been generated using the formulas presented in this paper.

Conflicts of interest

The author has no competing interests to declare. The author ensures that the work is entirely original.

References

1 N. S. Lloyd, J. Schwieters, M. S. A. Horstwood and R. R. Parrish, Particle detectors Used in Isotope Ratio Mass Spectrometry, with Applications in Geology, Environmental Science and Nuclear Forensics, in *Handbook of Particle Detection and Imaging*, ed. C. Grupen and I. Buvat, Springer-Verlag, Berlin Heidelberg, 2012.
2 S. Pommé and S. Boulyga, A throughput model explaining non-linearity in discrete ion counters used in mass spectrometry, *J. Anal. At. Spectrom.*, 2025, DOI: **10.1039/D5JA00085H**.
3 S. Pommé, Cascades of pile-up and dead time, *Appl. Radiat. Isot.*, 2008, **66**, 941–947.
4 S. Pommé, R. Fitzgerald and J. Keightley, Uncertainty of nuclear counting, *Metrologia*, 2015, **52**, S3–S17.
5 S. Richter, S. A. Goldberg, P. B. Mason, A. J. Traina and J. B. Schwieters, Linearity tests for secondary electron multipliers used in isotope ratio mass spectrometry, *Int. J. Mass Spectrom.*, 2001, **206**, 105–127.
6 U. Nygren, H. Ramebäck, M. Berglund and D. C. Baxter, The importance of a correct dead time setting in isotope ratio mass spectrometry: Implementation of an electronically determined dead time to reduce measurement uncertainty, *Int. J. Mass Spectrom.*, 2006, **257**, 12–15.
7 S. Richter, A. Alonso, Y. Aregbe, R. Eykens, F. Kehoe, H. Kühn, N. Kivel, A. Verbruggen, R. Wellum and P. D. P. Taylor, A new series of uranium isotope reference materials for investigating the linearity of secondary electron multipliers in isotope mass spectrometry, *Int. J. Mass Spectrom.*, 2009, **281**, 115–125.
8 U. Nygren, H. Ramebäck, A. Vesterlund and M. Berglund, Consequences of and potential reasons for inadequate dead time measurements in isotope ratio mass spectrometry, *Int. J. Mass Spectrom.*, 2011, **300**, 21–25.
9 S. Richter, S. Konegger-Kappel, S. F. Boulyga, G. Stadelmann, A. Koepf and H. Siegmund, Linearity testing and dead-time determination for MC-ICP-MS ion counters using the IRMM-072 series of uranium isotope reference materials, *J. Anal. At. Spectrom.*, 2016, **31**, 1647–1657.
10 M. Tanner and D. Günther, Short transient signals, a challenge for inductively coupled plasma mass spectrometry, a review, *Anal. Chim. Acta*, 2009, **633**, 19–28.
11 T. Nomizu, H. Hayashi, N. Hoshino, T. Tanaka, H. Kawaguchi, K. Kitagawa and S. Kaneco, Determination of zinc in individual airborne particles by inductively coupled plasma mass spectrometry with digital signal processing, *J. Anal. At. Spectrom.*, 2002, **17**, 592–595.
12 J. W. Olesik and P. J. Gray, Considerations for measurement of individual nanoparticles or microparticles by ICP-MS: determination of the number of particles and the analyte mass in each particle, *J. Anal. At. Spectrom.*, 2012, **27**, 1143–1155.
13 I. Strenge and C. Engelhard, Single particle inductively coupled plasma mass spectrometry: investigating nonlinear response observed in pulse counting mode and extending the linear dynamic range by compensating for dead time related count losses on a microsecond timescale, *J. Anal. At. Spectrom.*, 2020, **35**, 84–99.
14 M. Lomax-Vogt, L. M. Carter, J. Wielinski, S. Kutuzov, G. V. Lowry, R. Sullivan, P. Gabrielli and J. W. Olesik, Challenges in measuring nanoparticles and microparticles by single particle ICP-QMS and ICP-TOFMS: size-dependent transport efficiency and limited linear dynamic range, *J. Anal. At. Spectrom.*, 2025, **40**, 848–859.
15 H. Siegmund, S. Konegger-Kappel, S. Boulyga, M. Kilburn and S. Pommé, Recording high-intensity transient signals with secondary electron multipliers in MC-ICPMS: dead-time correction and non-linearity effects, 2025, in preparation.
16 G. Bédard, Dead-time corrections to the statistical distribution of photoelectrons, *Proc. Phys. Soc.*, 1967, **90**, 131–141.
17 M. C. Teich and W. J. McGill, Neural Counting and Photon Counting in the Presence of Dead Time, *Phys. Rev. Lett.*, 1976, **36**, 754–758.
18 G. Vanucci and M. C. Teich, Effects of rate variation on the counting statistics of dead-time-modified Poisson processes, *Opt. Commun.*, 1978, **25**, 267–272.
19 M. L. Larsen and A. B. Kostinski, Simple dead-time corrections for discrete time series of non-Poisson data, *Meas. Sci. Technol.*, 2009, **20**, 095101.

20 I. Strenge and C. Engelhard, Capabilities of fast data acquisition with microsecond time resolution in inductively coupled plasma mass spectrometry and identification of signal artifacts from millisecond dwell times during detection of single gold nanoparticles, *J. Anal. At. Spectrom.*, 2016, **31**, 135–144.
21 D. Mozhayeva and C. Engelhard, A critical review of single particle inductively coupled plasma mass spectrometry – A step towards an ideal method for nanomaterial characterization, *J. Anal. At. Spectrom.*, 2020, **35**, 1740–1783.
22 T. Hirata, S. Yamashita, M. Ishida and T. Suzuki, Analytical Capability of High-Time Resolution-Multiple Collector-Inductively Coupled Plasma-Mass Spectrometry for the Elemental and Isotopic Analysis of Metal Nanoparticles, *Mass Spectrom.*, 2020, **9**, A0085.
23 S. Yamashita, M. Ishida, T. Suzuki, M. Nakazato and T. Hirata, Isotopic analysis of platinum from single nanoparticles using a high-time resolution multiple collector Inductively Coupled Plasma - Mass Spectroscopy, *Spectrochim. Acta, Part B*, 2020, **169**, 105881.
24 T. Hirata, S. Niki, S. Yamashita, H. Asanuma and H. Iwano, Uranium-lead isotopic analysis from transient signals using high-time resolution-multiple collector-ICP-MS (HTR-MC-ICP-MS), *J. Anal. At. Spectrom.*, 2021, **36**, 70–74.
25 A. M. Duffin, E. D. Hoegg, R. I. Sumner, T. Cell, G. C. Eiden and L. S. Wood, Temporal analysis of ion arrival for particle quantification, *J. Anal. At. Spectrom.*, 2021, **36**, 133–141.
26 A. Hineman and C. Stephan, Effect of dwell time on single particle inductively coupled plasma mass spectrometry data acquisition quality, *J. Anal. At. Spectrom.*, 2014, **29**, 1252–1257.
27 P. Shaw and A. Donard, Nano-particle analysis using dwell times between 10 μs and 70 μs with an upper counting limit of greater than 3×10^7 cps and a gold nanoparticle detection limit of less than 10 nm diameter, *J. Anal. At. Spectrom.*, 2016, **31**, 1234–1242.
28 A. Schardt, J. Schmitt and C. Engelhard, Single particle inductively coupled plasma mass spectrometry with nanosecond time resolution, *J. Anal. At. Spectrom.*, 2024, **39**, 389–400.
29 S. Pommé, Radionuclide metrology: confidence in radioactivity measurements, *J. Radioanal. Nucl. Chem.*, 2022, **331**, 4771–4798.
30 S. Pommé, When the model doesn't cover reality: examples from radionuclide metrology, *Metrologia*, 2016, **53**, S55–S64.
31 International Commission on Radiation Units and Measurements (ICRU), Particle counting in radioactivity measurements, *ICRU Report*, Maryland, USA, 1994, vol. 52.
32 I. De Lotto, P. F. Manfredi and P. Principi, Counting statistics and dead-time losses, *Energ. Nucl.*, 1964, **11**, 557–564.
33 J. W. Müller, Sur l'arrangement en série de deux temps morts de types différents, *Internal Report BIPM*, Sèvres, France, BIPM-73/9, 1973.
34 J. W. Müller, Dead-time problems, *Nucl. Instrum. Methods*, 1973, **112**, 47–57.
35 J. W. Müller, Stastiques de comptage, *Internal Report BIPM*, Sèvres, France, BIPM-82/13, 1982.
36 J. Libert, Détermination du taux de comptage en amont de deux temps morts classiques en série et de types différents, *Nucl. Instrum. Meth. A*, 1989, **274**, 319–323.
37 S. Pommé, B. Denecke and J.-P. Alzetta, Influence of pileup rejection on nuclear counting, viewed from the time-domain perspective, *Nucl. Instrum. Meth. A*, 1999, **426**, 564–582.
38 S. Pommé, Time-interval distributions and counting statistics with a non-paralysable spectrometer, *Nucl. Instrum. Meth. A*, 1999, **437**, 481–489.
39 S. Pommé and G. Kennedy, Pulse loss and counting statistics with a digital spectrometer, *Appl. Radiat. Isot.*, 2000, **52**, 377–380.
40 S. Pommé and J. Uyttenhove, Statistical precision of high-rate spectrometry with a Wilkinson ADC, *J. Radioanal. Nucl. Chem.*, 2001, **248**, 263–266.
41 S. Pommé, Dead time, pile-up and counting statistics, in *Applied Modeling and Computations in Nuclear Science*, ACS Symposium Series, 2007, vol. 945, pp. 218–233.
42 S. Pommé and J. Keightley, Count rate estimation of a Poisson process - Unbiassed fit versus central moment analysis of time interval spectra. In: Applied Modeling and Computations in Nuclear Science, *ACS Symp. Ser.*, 2007, **945**, 316–334.
43 C. Michotte and M. Nonis, Experimental comparison of different dead-time correction techniques in single-channel counting experiments, *Nucl. Instrum. Meth. A*, 2008, **608**, 163–168.
44 S. Cheng, B. Pierson, S. Pommé and M. Flaska, Time interval distributions of nuclear events in a digital spectrometer, *Nucl. Instrum. Meth. A*, 2024, **1063**, 169218.
45 S. Pommé and K. Pelczar, A simplified approach to counting statistics with an imperfect pileup rejector, *Nucl. Instrum. Meth. A*, 2025, **1070**, 170067.
46 S. Cheng, B. Pierson, S. Pommé, B. Archambault and M. Flaska, Time-interval distributions in a digital gamma multi-channel analyzer at extreme input rates, *Nucl. Instrum. Meth. A*, 2025, **1073**, 170260.
47 R. Fitzgerald, Corrections for the combined effects of decay and dead time in live-timed counting of short-lived radionuclides, *Appl. Radiat. Isot.*, 2016, **109**, 335–340.
48 G. P. Westphal, Review of loss-free counting in nuclear spectroscopy, *J. Radioanal. Nucl. Chem.*, 2008, **275**, 677–685.
49 S. Pommé, J.-P. Alzetta, J. Uyttenhove, B. Denecke, G. Arana and P. Robouch, Accuracy and precision of loss-free counting in γ-ray spectrometry, *Nucl. Instrum. Meth. A*, 1999, **422**, 388–394.
50 S. Pommé, How pileup rejection affects the precision of loss-free counting, *Nucl. Instrum. Meth. A*, 1999, **432**, 456–470.
51 S. Pommé, Experimental test of the 'zero dead time' count-loss correction method on a digital gamma-ray spectrometer, *Nucl. Instrum. Meth. A*, 2001, **474**, 245–252.
52 S. Pommé, A plausible mathematical interpretation of the 'variance' spectra obtained with the DSPECPLUS TM digital spectrometer, *Nucl. Instrum. Meth. A*, 2002, **482**, 565–566.
53 S. Pommé, On the statistical control of 'loss-free counting' and 'zero dead time' spectrometry, *J. Radioanal. Nucl. Chem.*, 2003, **257**, 463–466.

